AIAA SciTech Forum
23-27 January 2023, National Harbor, MD & Online
AIAA SCITECH 2023 Forum

10.2514/6.2023-0825

Aeroelastic Analysis of Actuated Adaptive Wingtips Based on Pressure-Actuated Cellular Structures

Patrick Meyer* and Christian Hühne†
Technische Universität Braunschweig, 38106 Braunschweig, Germany

Kjell Bramsiepe‡ and Wolf Krüger§
German Aerospace Center (DLR), 37073 Göttingen, Germany

Folding wingtips are in the focus of research for their potential to counteract the challenges posed by high aspect ratio wings, such as airport conformity and increased wing root bending moment. Existing concepts for in-flight folding and morphing wingtips either enable passive load alleviation by adding free-flapping aeroelastic hinges to the wingtips or allow for advanced flight control and mission adaptability by actively deflecting the wingtips. In contrast, actuated adaptive wingtips combine the functionalities of passive and active in-flight folding wingtips by using a stiffness-adaptive aeroelastic hinge that is actively adjustable in flight. The objective of this paper is the aeroelastic analysis of a wing equipped with an adaptive-stiffness hinge. While the structural design of the wingtip actuator based on pressure-actuated cellular structures (PACS) was developed in a previous study, in this study the authors verify the concept of actuated adaptive wingtips through aeroelastic analysis. The aeroelastic model consists of a reduced beam structure coupled with the vortex lattice method. In the structural model, the PACS-based adaptive-stiffness hinge is implemented as an equivalent beam element and a pair of counteracting moments. This study shows that the investigated PACS actuator, which is structurally designed from glass-fiber reinforced plastic, is capable of bearing the loads acting on the wingtips of a Cessna Citation X. The adaptive-stiffness hinge, positioned between 86.7% and 91.2% of the semi-span, reduces the wing root bending moment by up to 7.8% in a 2.5 g maneuver load case, while keeping the wing straight in cruise. A further increase in load alleviation potential can be achieved in the future by extending the actuator's operating envelope and thus increasing its load-bearing capacity so that the actuator can be positioned more inboard. The functional verification of the actuated adaptive wingtip concept by means of aeroelastic analysis forms the basis for the manufacturing and testing of a functional prototype.

Nomenclature

E	=	modulus of elasticity	n_z	=	load factor
EI	=	bending stiffness	p_h	=	pressure in the row of hexagonal cells
GI_T	=	torsional stiffness	p_t	=	pressure in the row of tetragonal cells
h	=	height	R	=	material strength
k	=	actuator stiffness	w	=	width
L	=	wing lift distribution	y	=	spanwise coordinate
l	=	length	z	=	wing deflection
M	=	actuator moment	β	=	angular deflection of the actuator
M_b	=	wing bending moment	Θ	=	wing twist

*Research associate and doctoral student, Institute of Mechanics and Adaptronics, Langer Kamp 6, pat.meyer@tu-braunschweig.de, AIAA member.
†Professorship for function integration, Institute of Mechanics and Adaptronics, Langer Kamp 6, christian.huehne@tu-braunschweig.de.
‡Research associate and doctoral student, Institute of Aeroelasticity, Bunsenstr. 10, kjell.bramsiepe@dlr.de.
§Professor and head of division loads analysis and design, Institute of Aeroelasticity, Bunsenstr. 10, wolf.krueger@dlr.de.

I. Introduction

Increasing the aspect ratio of transport aircraft significantly reduces the aircraft's induced drag, leading to a reduction in fuel burn and noise emissions [1]. However, increasing the wingspan is accompanied by three disadvantages: First, the aircraft's wingspan is restricted by airport operating rules, regulated by the Aerodrome Reference Code [2] of the International Civil Aviation Organization (ICAO) or the Airplane Design Group [3] of the Federal Aviation Administration (FAA). Second, the wing root bending moment (WRBM) increases with the wing's aspect ratio. Consequently, the wing structure must be reinforced, which is associated with additional structural mass and hence with additional loads. Third, increasing the wingspan reduces the aircraft's maneuverability, especially the roll authority, assuming the control surface layout remains unchanged. Moving the ailerons further outboard is not feasible with current actuator technologies due to the limited installation space at the tip of slender high aspect ratio (HAR) wings. Moreover, slender flexible wings lead to higher deformations reducing the effectiveness of ailerons. To avoid control reversal, constraints regarding the control surface efficiency must be taken into account [4] affecting the structural design.

An effective way to comply with on-ground size restrictions are folding wings. Carrier-based aircraft have been equipped with folding wings for decades to meet extreme storage requirements, such as the Grumman F4F-4 Wildcat developed in 1941 [5]. Folding wings have recently found their way into commercial aviation. The Boeing 777X, having made its first flight in 2020, is equipped with folding wingtips (FWT). With its wingtips folded upwards on ground, the aircraft meets the 65 m wingspan limit of the ICAO Aerodrome Reference Code letter E, allowing the same gates to be used as with the original Boeing 777. During taxiing, the pilot unfolds and locks the wingtips of the 777X, increasing the wingspan by 7 m, i.e. 10%, in flight [6]. Instead of folding the wingtips upwards, Airbus invented a downwards folding mechanism [7]. Downward folding has the advantage of resulting in a lighter mechanism, as the lift acts against the folding direction. However, all folding mechanisms are accompanied by increased system complexity and additional weight caused by the actuation mechanism.

While on-ground FWT allow for increasing the aircraft's wingspan, in-flight FWT allow for adapting the wing's lift coefficient to changing flight conditions, enabling new functionalities and efficiency gains. Ajaj et al. [8] show that there is considerable recent interest in out-of-plane morphing, including wingtip folding and bending, for large transport aircraft. Passive in-flight FWT enable passive load alleviation and roll damping alleviation, whereas active in-flight FWT allow mission adaptability, active load alleviation and advanced flight control [9]. A recent example of passive in-flight FWT is the Airbus AlbatrossONE flight demonstrator, built to investigate free-flapping wingtips with aeroelastic hinges enabling passive load alleviation. Flight tests with the AlbatrossONE were performed in 2019 [10] and 2020 [11] proofing the concept of the semi aeroelastic hinge (SAH). The SAH is being further explored on a larger scale with Airbus' extra performance wing demonstrator (X-Wing), whose platform is based on a Cessna Citation VII business jet [12].

Examples of aircraft equipped with active in-flight FWT are the XB-70 Valkyrie [13] or NASA's prototype-technology evaluation and research aircraft (PTERA) [14]. By slowly adapting their wing shape in flight by folding the wingtips, they improve the aircraft's aerodynamics during changing flight conditions. In contrast to slow wingtip actuation, fast asymmetric wingtip deflections enable advanced flight control by generating roll moment. So far, actuated wingtips used as control surfaces have only been investigated for unmanned aerial vehicles (UAV) and small-scale aircraft, such as in the experimental study of Mills et al. [15], in which actuated wingtips are implemented as control effectors on a mini-UAV with a conventional aircraft configuration. A detailed review on in-flight folding and morphing wingtips is presented in [9].

The combination of the functionalities of passive and active FWT in one single system requires a stiffness-adaptive wingtip with an aeroelastic hinge that is actively adjustable in flight. This combined system is referred to by the authors as *actuated adaptive wingtips* [9]. An adaptive shape of the wingtips allows mission adaptability, advanced flight control, active load alleviation, and airport conformity of HAR wings, whereas adaptive stiffness of the wingtips allows advanced passive load alleviation. In addition, only a continuous deformation of the wingtip, i.e. a morphing structure without discrete hinges, results in efficient aerodynamics.

The concept of actuated adaptive wingtips presented in this study is based on pressure-actuated cellular structures (PACS), which can be used as actuators for large morphing structures demanding adaptive stiffness and continuous shape [16]. Figure 1 shows a schematic representation of an aircraft equipped with actuated adaptive wingtips using PACS actuator technology. PACS, first studied by Pagitz et al. [17], consist of multiple rows of polygonal cells with rigid walls and flexible hinge areas. By changing the cell pressurization, the structural stiffness and global deflection of PACS actuators can be adjusted simultaneously. While the actuator's deflection depends on the pressure difference between the individual cell rows, the actuator's stiffness depends on the total pressurization of all cells. These properties make PACS an ideal candidate for actuated adaptive wingtips.

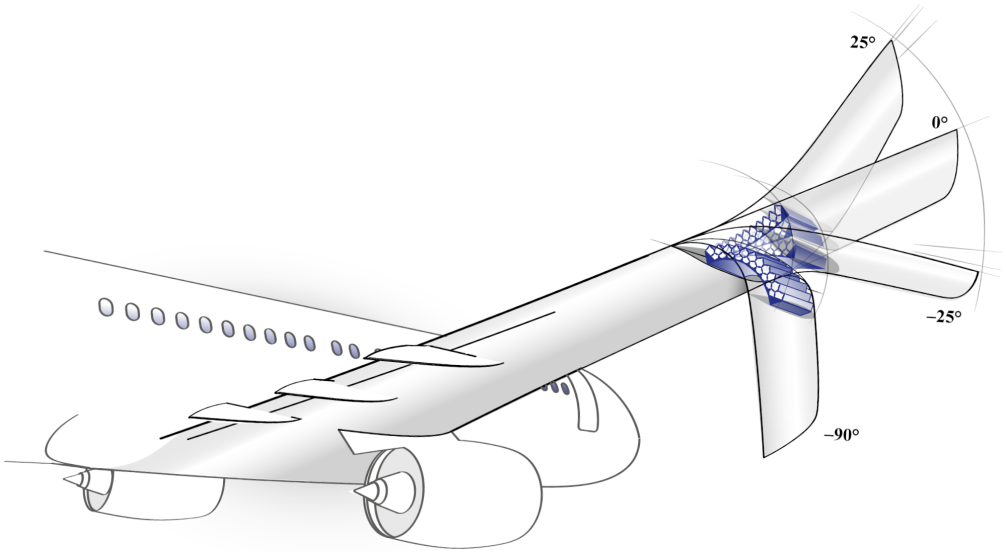

Fig. 1 Schematic representation of actuated adaptive wingtips based on pressure-actuated cellular structures (PACS).

The load-bearing capacity and the adaptive-stiffness characteristics of a PACS actuator were identified in [9], using a preliminary design of an actuated adaptive wingtip. Based on an in-depth functional analysis, the authors defined requirements for in-flight morphing wingtip devices and investigated the limitations of the PACS actuator technology at the example of a HAR mid-range transport aircraft with a 55 m span. A finite element analysis (FEA) showed that the PACS actuator meets the required deflection angles for airport conformity, roll control, mission adaptability, and active load alleviation. In addition, the adaptive stiffness of the actuator enables passive load alleviation. However, the investigated actuator design has limited load-bearing capacity due to very localized stress peaks and cannot withstand the moments acting on the wingtips of the 55 m span mid-range transport aircraft. Nevertheless, the results show that the load-bearing capacity of the investigated PACS actuator, i.e. the maximum moment the actuator can apply without structural failure, exceeds that of other wingtip actuators used on small-scale flight demonstrators, like the PTERA flight demonstrator [14] or the UAV studied in [15].

This paper investigates actuated adaptive wingtips based on PACS on an aircraft similar in size to a Cessna Citation X. The Cessna Citation X is selected due to the availability of the required aircraft data and for comparability with current research, such as Airbus' X-Wing project [12]. The actuator's stiffness profile determined in [9] is used as a basis for the aeroelastic characterization of actuated adaptive wingtips. The objective of this paper is the aeroelastic analysis of a wing equipped with an adaptive-stiffness hinge. The wing's deflection, twist, lift, and bending moment distributions in cruise flight and maneuver load cases are then compared with those of the reference wing without wingtip actuator.

The paper is structured as follows: Section II reviews requirements for actuated adaptive wingtips and describes the adaptive-stiffness characteristics of a PACS-based wingtip actuator, which is then implemented on the wingtips of a Cessna Citation X (Section III). The aeroelastic model of an adaptive-stiffness wing is presented in Section IV, whereas Section V shows the results of the aeroelastic analysis. Section VI compares the actuated adaptive wingtip concept with other wingtip devices and discusses the advantages and challenges of PACS actuators, while Section VII summarizes this paper and highlights future research.

II. Actuated Adaptive Wingtips Based on PACS

In this paper, the aeroelastic behavior of actuated adaptive wingtips is characterized. The investigated actuator is based on the PACS actuator technology that enables adaptive stiffness and continuous shape morphing. The presented PACS actuator is initially designed for a HAR mid-range transport aircraft as described in [9]. This section summarizes the requirements for HAR wings equipped with actuated adaptive wingtips, the working principle of PACS actuator technology, the actuator design, and its mechanical characteristics.

A. Requirements for Actuated Adaptive Wingtips

Requirements for multifunctional actuated adaptive wingtips for improving aircraft performance and efficiency are identified in [9]. Table 1 provides an overview of the design features of actuated adaptive wingtips and how they affect the functional requirements of HAR aircraft. The table shows that the combination of four design features covers all requirements. These features are variable span, dynamic actuation, stiffness adaptivity, and continuous shape morphing. Actuated adaptive wingtips using PACS actuators provide all four functional features and thus cover all specified requirements.

Table 1 Functional requirements and design features of actuated adaptive wingtips [9].

Feature →	Span			Wingtip hinge					Contour		
↓ Requirement:	Short	Large	Variable	Rigid	Flexible	Stiffness-adaptive	Actuated (quasi-static)	Actuated (dynamic)	Discrete	Semi-continuous	Continuous
Airport conformity	+	−	+								
Low WRBM	+	−	+								
Roll authority	+	−	+								
Low induced drag	−	+	+								
Flight stability				+	−	+	○	○			
Mission efficiency				−	−	−	+	+			
Passive load alleviation				−	+	+	−	−			
Active load alleviation				−	−	−	−	+			
Flight control				−	−	−	−	+			
Aerodynamic efficiency									−	○	+

Design feature affects the functional requirement: positive (+), neutral (○), negative (−)

B. Working Principle of PACS Actuators

The biomimetic working principle of PACS mimics the nastic movement of plants. Representative examples of plants performing nastic movements are the Venus flytrap (*Dionaea muscipula*) or the sensitive plant (*Mimosa pudica*), which fold their leaves by varying the cells' turgor pressure. This change in turgor pressure in combination with flexible cell walls allows the plants to move their leaves without the presence of muscles or rigid-body mechanisms.

Transferring the pressure-based deformation of plants to an engineering system results in a cellular structure consisting of multiple rows of polygonal cells with rigid cell walls and flexible hinge areas [17]. An increase in cell pressure causes a deformation of each cell into a state of minimal internal energy, which occurs when all hinges lie on a circular arc and the cross-sectional area becomes maximum. Any further increase in pressure no longer changes the cells' geometry but stiffens the structure. The ratio of the cell wall lengths determines the maximum deflection of each individual cell. The sum of all cell deformations consequently determines the total deflection of the cellular structure. By changing the cell pressure, the structural stiffness and global deflection of PACS actuators can be adjusted simultaneously. The actuator's deflection depends on the pressure difference between the individual cell rows, whereas the actuator's stiffness depends on the total pressurization of all cells.

A geometry optimization algorithm allows the design of polygonal cellular structures that move between two predefined target shapes. The basis for the geometry optimization algorithm is a pseudo-rigid-body model (PRBM) [18] for representing PACS that consist of rigid cell walls connected by small-length flexural pivots (SLFP). The SLFP are modeled by discrete pin joints and torsion springs with an equivalent hinge stiffness. The geometry optimization

algorithm applies the principle of virtual work that allows calculating the structure's pressure-dependent state of equilibrium. Using this algorithm, the length of each cell wall is iteratively adjusted until the deformed shapes match the predefined target shapes at given external loads and cell pressures. Subsequently, the PRBM is translated into a cross-sectional design, considering cell wall geometries and replacing the pin joints with flexure hinges. A comprehensive description of the holistic design approach of PACS is presented by Gramüller et al. [19].

C. Actuator Design

A preliminary design of a PACS actuator was conducted in [9] for a HAR mid-range transport aircraft with 55 m wingspan, considering the requirements for actuated adaptive wingtips presented in Table 1. Based on the structural design from [9], this study investigates the aeroelastic behavior of a wing equipped with that PACS actuator. This subsection summarizes the steps necessary when designing PACS and presents the geometric model of the PACS actuator.

The design steps include selecting the topology of the actuator, the mechanical dimensioning of the cell walls and hinges, the determination of its cross-sectional geometry, and verification by means of FEA. Figure 2 shows the cross-sectional geometry of the designed actuator consisting of two rows of hexagonal and tetragonal cells, and its deformed shapes. The number of hexagonal and tetragonal cells is 11 and 10. A glass-fiber reinforced plastic is used featuring a high squared strength to modulus ratio (R^2/E), which is a prerequisite for high-performance compliant mechanisms. The required deflections of the wingtip, i.e. the variations in cant angle, define the maximum angular deflections β_{min} and β_{max} of the actuator. The actuator is designed to allow a variation in cant angle between $-90°$ and $25°$. All design parameters used as input values for the PACS geometry optimization are described in detail in [9].

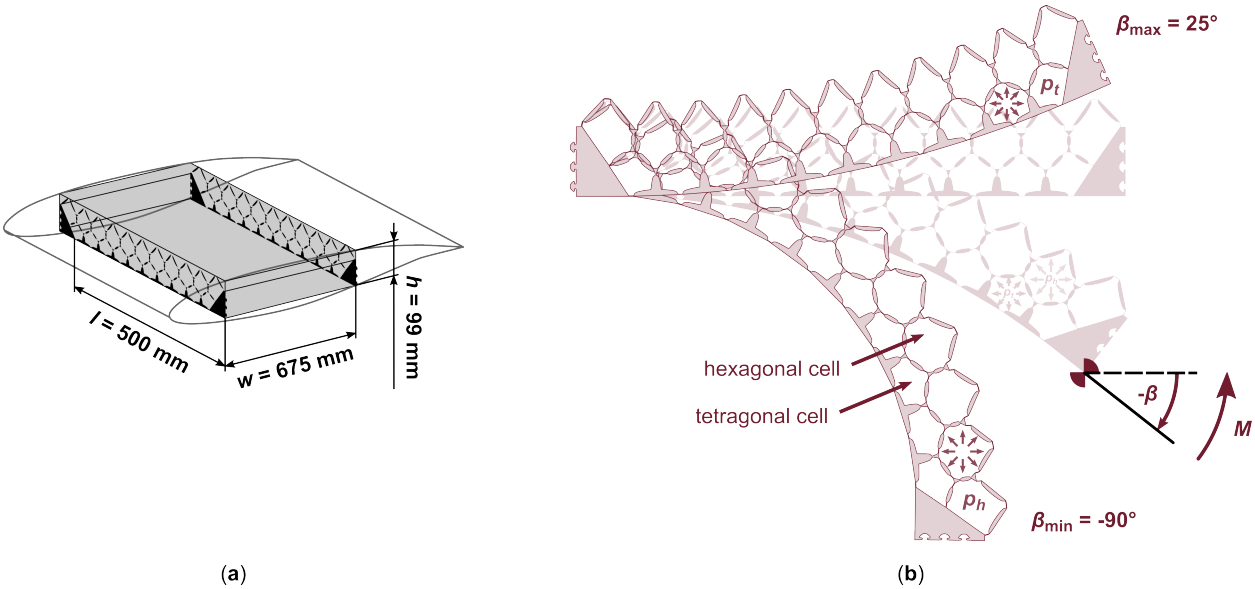

Fig. 2 Geometric model of the PACS actuator: (a) The size of the actuator is $l = 500$ mm, $h = 99$ mm and $w = 675$ mm. (b) Definition of cell row pressures p_t and p_h, angular deflection β, and counteracting moment M.

D. Actuator Characteristics

The shape-adaptive and stiffness-adaptive actuator characteristics are determined by means of high-fidelity FEA using the simulation software ANSYS. A large set of data points is generated for different combinations of cell pressures p_t and p_h, and external moments M in order to determine the actuator's operating envelope restricted by the material strength. The main outcome of the actuator characterization described in [9] is presented in Fig. 3.

The feasible domain of cell pressures is limited by structural stresses caused by distortion of the flexure hinges. Figure 3 (a) shows the interpolated active stress restriction as a function of the cell pressures p_t and p_h at different angular deflections β. Structural failure occurs due to stress peaks in the transition region between the rigid walls and the flexure hinges. The very localized stress peaks imply that form optimization of the flexure hinges could significantly

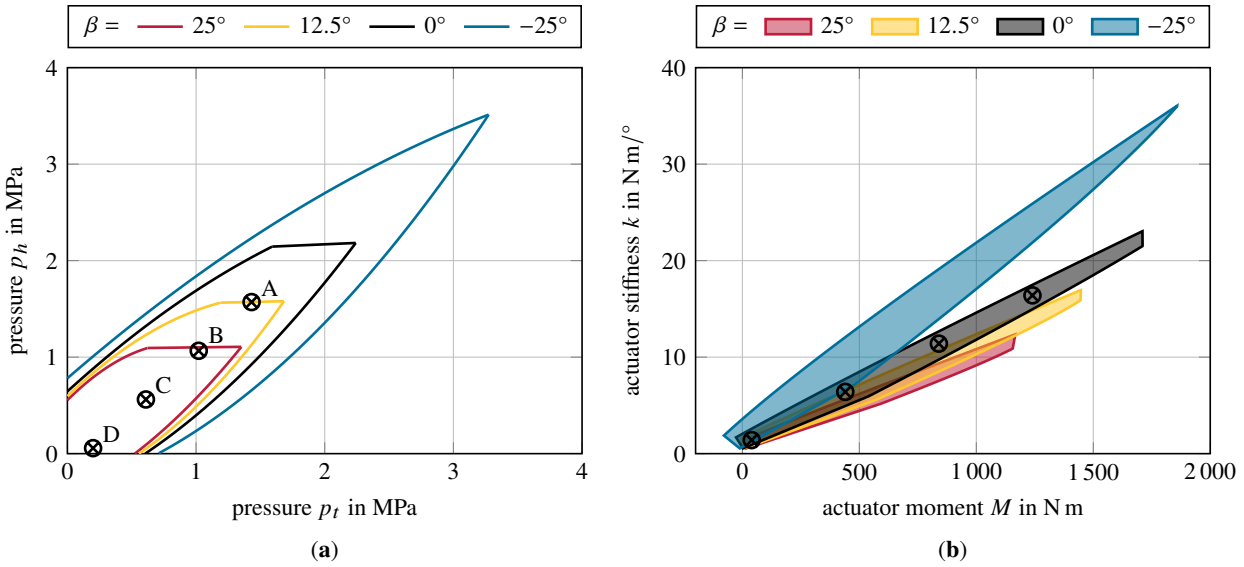

Fig. 3 Comparison of the PACS actuator characteristics at angular deflections of $\beta = 25°$, $\beta = 12.5°$, $\beta = 0°$ and $\beta = -25°$: (a) Operating envelope limited by the material strength defining valid pressure states. (b) Feasible domain of actuator stiffnesses k at a given moment M. The markers indicate the pressure states and associated actuator stiffnesses used in the aeroelastic model.

extend the feasible pressure domain leading to a higher load-bearing capacity of the actuator.

For each pressure state, the actuator's rotational stiffness k is determined by the ratio of tip moment M to angular deflection β. The actuator stiffness mainly depends on the cell pressures p_t and p_h and its linear prediction function is given by

$$k = 1.89\,\mathrm{N\,m/(^\circ\,MPa)} \cdot p_t + 8.37\,\mathrm{N\,m/(^\circ\,MPa)} \cdot p_h + 0.55\,\mathrm{N\,m/^\circ}. \tag{1}$$

The bending moment applied by the actuator

$$M = k \cdot \beta + M_{\beta=0^\circ} \tag{2}$$

is determined by its stiffness k and the moment at zero angular deflection $M_{\beta=0^\circ}$, whose linear prediction function is defined by

$$M_{\beta=0^\circ} = -49.2\,\mathrm{N\,m/MPa} \cdot p_t + 832.6\,\mathrm{N\,m/MPa} \cdot p_h + 2.6\,\mathrm{N\,m}. \tag{3}$$

With Eq. (1) and Eq. (2), the feasible domain of actuator stiffnesses k and moments M for different angular deflections β is determined using the cell pressures forming the active stress restriction envelopes in Fig. 3 (a). Figure 3 (b) shows the feasible domain of actuator stiffnesses k for a given moment M at different angular deflections β. The presented PACS actuator shows significant stiffness adaptivity and a maximum zero-deflection moment of $M_{\beta=0^\circ} = 1711\,\mathrm{N\,m}$ in cruise conditions. At a constant external moment, the actuator stiffness can be varied between the upper and lower boundary of its feasible domain without changing the angular deflection β.

Adapting the actuator's stiffness allows for a tailored load alleviation capability. While a high stiffness maintains the wing shape in cruise, a reduced stiffness enhances load alleviation in gust and maneuver scenarios. The markers in Fig. 3 indicate four different pressure states and associated actuator stiffnesses for operating the PACS actuator in an active load alleviation mode. The selected pressure states are listed in Table 2 and their stiffness values are used in the aeroelastic analysis described below. All selected pressure states are within the stress restriction envelope of $\beta = 12.5°$. Therefore, any wingtip deflection of $\beta \leq 12.5°$ is permissible when operating in this mode. Pressure state "A" coincides with the stress restriction boundary and is therefore limited to $\beta = 12.5°$, whereas higher angular deflections are possible by actively reducing the actuator stiffness (pressure states "B" to "D"). Pressure state "D" represents an almost zero-stiffness hinge and all other pressure states are linearly interpolated between pressure state "A" and pressure state "D".

Table 2 Pressure states and associated actuator stiffnesses and moments.

State	Cell pressures		Actuator moment	Actuator stiffness
	p_t	p_h	M	k
A	1.43 MPa	1.57 MPa	1240 N m	16.4 N m/°
B	1.02 MPa	1.07 MPa	840 N m	11.4 N m/°
C	0.61 MPa	0.56 MPa	440 N m	6.4 N m/°
D	0.20 MPa	0.06 MPa	40 N m	1.4 N m/°

III. Reference Aircraft and Actuator Integration

A. Aircraft Selection: Cessna Citation X

The mechanical actuator characterization reveals that the PACS actuator with its current design can apply a maximum zero-deflection moment of $M_{\beta=0^\circ} = 1711$ N m in cruise conditions. The previous study [9] found that this is below the required moment acting on the wingtip of a 55 m span HAR mid-range transport aircraft by a factor of 8.8. However, it is estimated that the load-bearing capacity of the PACS actuator is of the same order of magnitude as the loads encountered on the wingtips of smaller aircraft.

Current research activities investigating in-flight folding and morphing wingtips are performed on aircraft similar in size to common business jets and regional aircraft with a span in the range of 15 m to 20 m. Segui et al. [20] conducted aerodynamic studies on a modified Cessna Citation X by adding winglets with variable dihedral. They showed that adding winglets to a Cessna Citation X improves the fuel consumption in cruise by up to 2.1% compared to the original aircraft without winglets. In addition, Segui et al. [21] investigated adaptive winglets on a Bombardier CRF700 regional aircraft. The results show an increase in lift-to-drag ratio of up to 6.1% by adapting the winglet's cant angle compared to the baseline winglet configuration with a cant angle of 73°. Recently, Airbus announced the X-Wing project that will investigate implementing an aeroelastic hinge on a Cessna Citation VII flight demonstrator with approximately 16 m span (representing a 30% model of a 52 m span aircraft) and with a 2 m long movable tip section [22].

Therefore, in accordance with these research activities, the reference aircraft selected for the aeroelastic analysis of actuated adaptive wingtips based on PACS is a Cessna Citation X with 19.38 m span. The Cessna Citation X is also selected due to the availability of the required aircraft data. Table 3 shows the main characteristics of the reference aircraft used in the aeroelastic model. The data are adapted from the study of Segui et al. [20]. The wing area and aspect ratio in the table differ slightly from the actual values of the Cessna Citation X because the segmented trapezoidal wing planform is not included in the aeroelastic model described below. Figure 4 shows the Cessna Citation X and the wing planform used in the aeroelastic model.

Table 3 Main characteristics of the reference aircraft.

Parameter	Symbol	Value
Span	b	19.38 m
Wing sweep	φ	36.0°
Wing area	A_w	54.65 m^2
Aspect ratio	AR	6.87
Root chord	c_R	4.85 m
Tip chord	c_T	0.81 m
Actuator position	η_{PACS}	86.7% to 91.2%
Actuator length	l_{PACS}	0.5 m

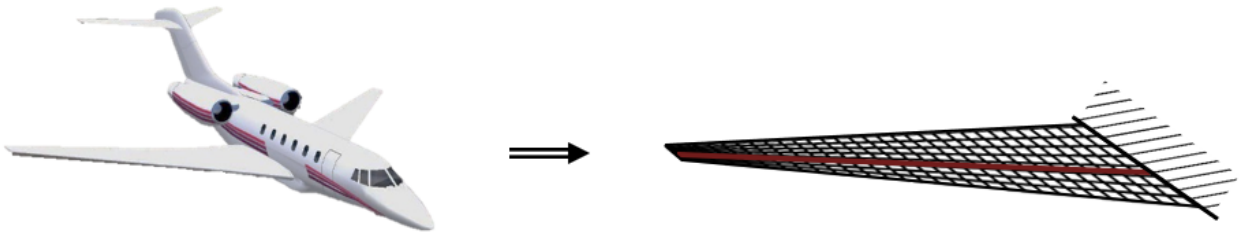

Fig. 4 Cessna Citation X and simplified aeroelastic model of the clamped wing.

B. Positioning of the PACS Actuator

The spanwise position of the PACS actuator is defined by the local wing bending moment and the maximum zero-deflection moment $M_{\beta=0^\circ}$ of the actuator. To achieve a straight wing shape in cruise, the moment applied by the actuator must counteract the local wing bending moment. The actuator position is determined in an initial aeroelastic analysis for an actuator moment of $M_{\beta=0^\circ} = 1240\,\mathrm{N\,m}$, corresponding to pressure state "A" in Table 2. According to the analysis, the 0.5 m long PACS actuator is positioned between 86.7% and 91.2% of the semi-span. Thus, approximately 10% of the semi-span is actuated, which is a reasonable trade-off between loads and performance, as recommended in [23].

The bending axis of the actuator is oriented perpendicular to the wing's leading edge, resulting in an outwards-pointing hinge line with a flare angle of 36°, which is identical to the sweep angle of the wing. Using a non-zero hinge-line angle with respect to the free stream direction significantly improves the load alleviation capability since upward folding of the wingtip is then associated with a reduction of the local angle of incidence [24, 25].

IV. Aeroelastic Model

To investigate the aeroelastic effects of the stiffness-adaptive wingtip concept based on PACS, an aeroelastic method is utilized. The method is capable of analyzing multilinear elastic stiffnesses and adaptive stiffnesses and is based on a reduced beam structure coupled with the vortex lattice method (VLM). For the latter, the VLM implemented in the *Loads Kernel* tool is used [26, 27]. The structural analysis is performed with beam elements implemented in a Python routine, which was verified with MSC.Nastran [28].

Three model variants are considered in the aeroelastic analysis. First, a wing similar to that of the Cessna Citation X without wingtip actuator is examined as a reference. Then, two cases of a wing with an integrated PACS actuator are investigated. The actuator can be operated in a passive or active mode, where in active mode the stiffness is reduced with increasing loads.

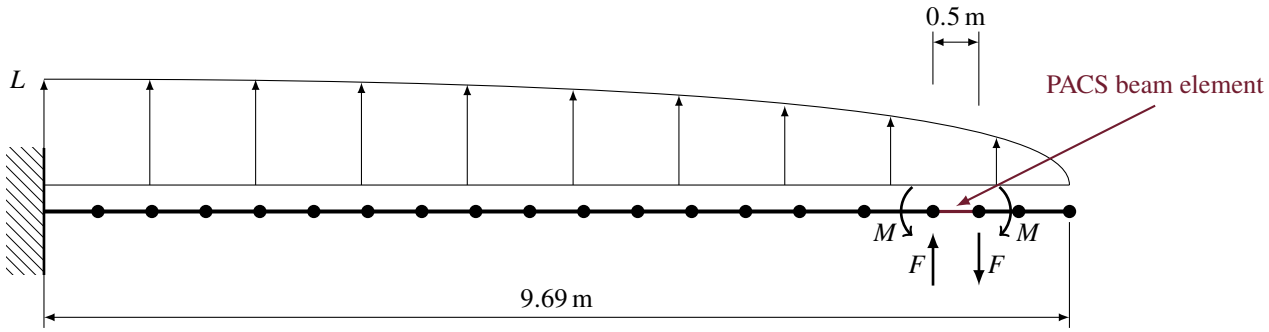

Fig. 5 Concept sketch of the aeroelastic model of a wing with an integrated PACS actuator.

The structural model of the wing consists of a beam structure instead of a high-fidelity model with shell elements to reduce the modeling effort of new technologies [28]. Figure 5 illustrates a concept sketch of the structural elements used in the aeroelastic model. The model discretization uses beam elements with an element length of 0.51 m, resulting in a total of 19 elements representing the wing structure. The beam properties of the reference wing are calculated from the estimated wing box dimensions of the Cessna Citation X given in Table 4 and using the material properties

of aluminum. The spanwise distribution of the wing bending stiffness EI_{wing} and the torsional stiffness $GI_{T,\text{wing}}$ are linearly interpolated between the values at the root and the tip. So, kinks and other geometric structural variations are neglected.

Table 4 Wing box dimensions similar to those of a Cessna Citation X used in the structural model.

Parameter	Symbol	Value at root	Value at tip
Width	w_{box}	2.66 m	0.45 m
Height	h_{box}	0.48 m	0.06 m
Skin thickness	t_{skin}	8 mm	2 mm
Spar thickness	t_{spar}	5 mm	2 mm
Beam stiffness	EI_{wing}	$183.6 \cdot 10^6$ N m^2	$0.182 \cdot 10^6$ N m^2

The aerodynamic model with the simplified trapezoidal wing used in the VLM is shown in Fig. 4. To calculate the aerodynamic loading with VLM, the wing shape is divided into a grid of 8×30 equidistant panels. The loads are calculated for four different load factors n_z varying from 1.0 to 2.5 with the conditions given in Table 5, which are representative of the cruise and design load cases of the Cessna Citation X. The aerodynamic forces are transferred to the structure by rigid body elements. These elements are created between the nodes of the aerodynamic grid and those nodes of the structural grid which have the smallest distance, respectively. Then, the wing deformation and the corresponding loads are determined with an iterative trim analysis of the angle of attack.

Table 5 Load conditions investigated in the aerodynamic model.

Parameter	Symbol	Value
Flight level	FL	300 (9144 m)
Velocity	v_{TAS}	270.0 m/s
Mach number	Ma	0.89
Maximum take-off mass	MTOM	16.4 t
Load factors	n_z	1.0, 1.5, 2.0 and 2.5

When modeling the wing with the integrated PACS actuator, the stiffness properties of one beam element in the structural model are replaced by the stiffness characteristics of the PACS actuator. The PACS actuator is characterized by its rotational stiffness k, but the aeroelastic model consists of beam elements defined by a bending stiffness EI. Therefore, the rotational stiffness is converted into an equivalent beam stiffness $EI_{\text{PACS}} = k \cdot l_{\text{PACS}}$ using the length of the actuator segment $l_{\text{PACS}} = 0.5$ m. Figure 6 (a) schematically shows the PACS actuator integrated into the wingtip of the Cessna Citation X, whereas Fig. 6 (b) shows the equivalent PACS beam element used in the aeroelastic model.

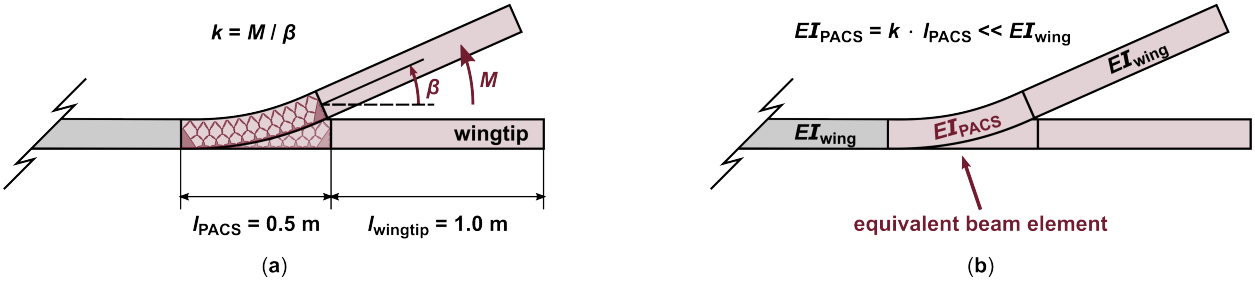

Fig. 6 Implementation of the PACS actuator in the aeroelastic model: (a) PACS actuator integrated into the wingtip of the Cessna Citation X and (b) its representation as an equivalent beam element. The wing bending stiffness EI_{wing} decreases linearly from the root to the tip.

The equivalent PACS beam element can be changed in stiffness and additional loading. Different actuator stiffnesses, i.e. different pressure states, cause positive or negative deflection of the PACS actuator. The initial deflection of the PACS actuator due to its pressurization can be represented in the beam model by applying a preload. To model this initial deflection, a pair of moments and a pair of shear forces are added at the nodes of the PACS beam element, as shown in Fig. 5. The pair of moments and the pair of shear forces add up to the given actuator moments in Table 6.

The PACS actuator can be operated in passive and active modes. In the passive mode, the stiffness and moment of the actuator are kept constant. The passive mode corresponds to pressure state "A" in Fig. 3 and Table 2. In the active mode, the actuator features a degressive stiffness behavior. While the stiffness is identical to the passive mode in cruise flight ($n_z = 1.0$), the stiffness is actively reduced with increasing load factor. As the load factor increases, the stiffness of the actuator decreases linearly (pressure states "B" and "C" in Fig. 3) until almost zero in the 2.5 g maneuver load case (pressure state "D"). Table 6 assigns the actuator stiffnesses and counteracting moments to the respective operating modes and load conditions. When comparing the stiffnesses EI_{PACS} of the PACS beam element to the stiffness EI_{wing} of the reference wing as given in Table 4, the stiffness ratio is less than 0.1%.

Table 6 Stiffness and moment variations of the PACS actuator operated in passive and active mode.

Mode	Load factor n_z	Pressure state (Fig. 3)	Actuator moment M	Actuator stiffness k	Beam stiffness EI_{PACS}
Passive	All	A	1240 N m	16.4 N m/°	469.8 N m^2
Active	1.0	A	1240 N m	16.4 N m/°	469.8 N m^2
	1.5	B	840 N m	11.4 N m/°	326.6 N m^2
	2.0	C	440 N m	6.4 N m/°	183.3 N m^2
	2.5	D	40 N m	1.4 N m/°	40.1 N m^2

V. Results of the Aeroelastic Analysis

The static aeroelastic analysis determines the deflection, twist, lift, and bending moment distributions for an aircraft wing similar to that of a Cessna Citation X. Figure 7 shows the results of the aeroelastic analysis, whereas Table 7 summarizes the main results. Three model variants and four load cases each are considered. The model variants represent the reference wing without wingtip actuator (black lines), and the wing with integrated PACS actuator operating in passive mode (red lines), and in active mode (blue lines).

Figure 7 (a) shows the wing deflection for all investigated cases. The wing deflection of the 1.0 g cruise flight (dotted lines) is almost identical for all three model variants because the moment applied by the actuator compensates for the locally reduced stiffness and maintains the straight wing shape in cruise. It follows that the twist, lift, and bending moment distributions in cruise are also identical for all three model variants (Fig. 7 (b) to Fig. 7 (d)). However, for the 1.5 g maneuver (dash-dotted lines), the 2.0 g maneuver (dashed lines), and the 2.5 g maneuver (solid lines) the wing deflection increases considerably at the position of the adaptive-stiffness hinge.

The upward folding of the wingtip for $n_z > 1.0$ is followed by a step in the wing twist distribution, as shown in Fig. 7 (b). The step in the wing twist is due to the bending–torsion coupling of backward-swept wings since the hinge line is perpendicular to the wing's leading edge and not parallel to the flow. The outwards-pointing hinge line of the wingtip actuator amplifies the reduction of the wingtip's angle of incidence.

The reduction of the wingtip's angle of incidence causes washout of the lift distribution, shifting the lift towards the inner wing, as shown in Fig. 7 (c). The lift distribution of the adaptive-stiffness wing is reduced outboard of the hinge and increased inboard. The washout effect is most pronounced for the adaptive-stiffness hinge operated in active mode. Table 7 shows that the lift generated by the wingtip of the model variant with PACS operated in passive mode is nearly constant for all load factors, whereas the wingtip lift of the reference wing increases significantly with increasing load factor. When operating PACS in active mode, the wingtip lift reduces to almost zero in the 2.5 g maneuver load case.

The inboard shift of the lift distribution results in a bending moment reduction over the entire span of the wing (Fig. 7 (d)). The reduction in bending moment allows the design of a lighter wing or an increase in payload. Table 7 shows the relative reduction in WRBM for each load factor when comparing the PACS model variants to the reference wing. The adaptive-stiffness hinge reduces the WRBM in a 2.5 g maneuver by 4.2% in passive mode and by 7.8% in

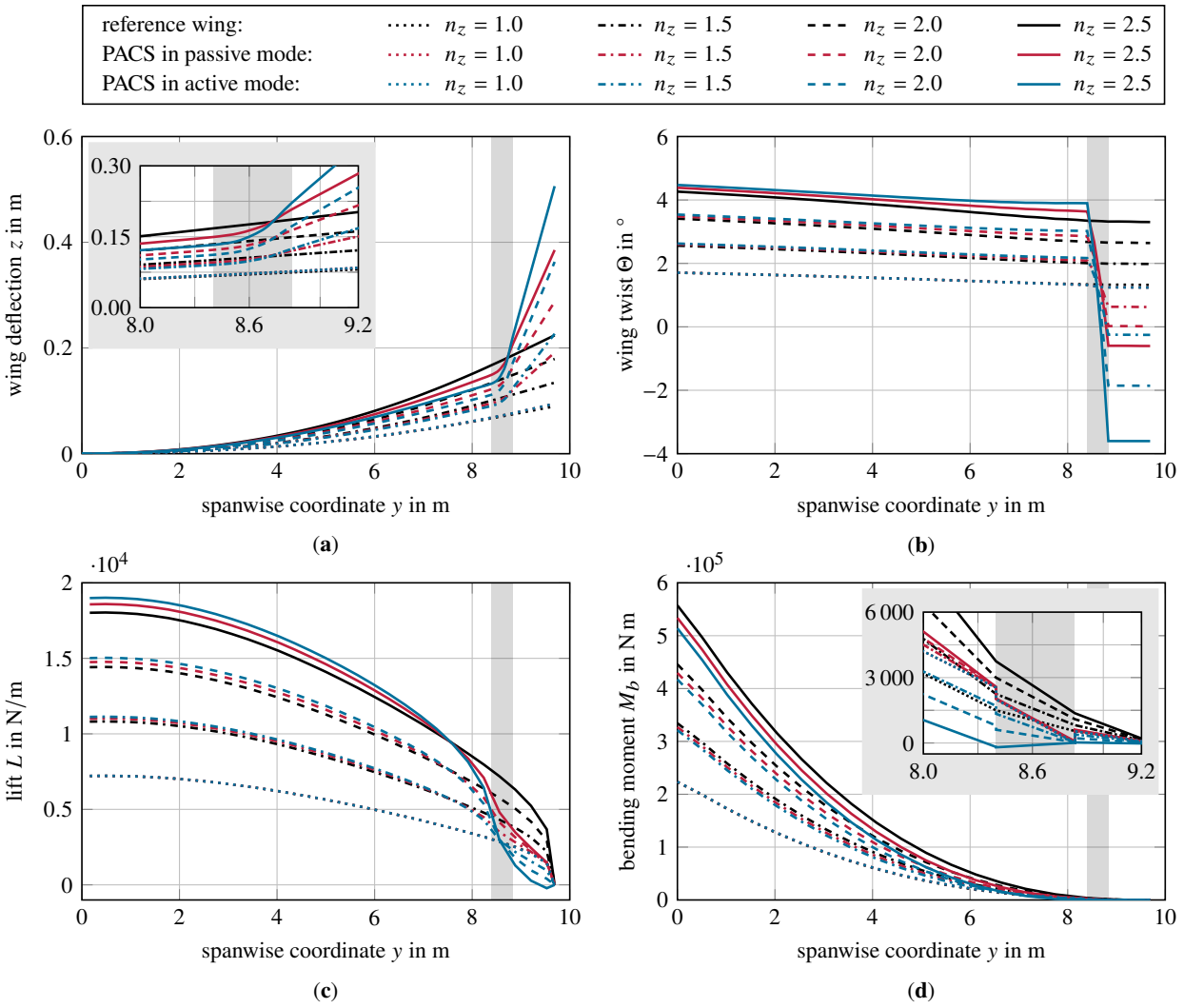

Fig. 7 Wing deflection, twist, lift, and bending moment distributions of the Cessna Citation X with an adaptive-stiffness hinge between 86.7% and 91.2% of the semi-span for different load factors n_z.

active mode. The detailed view of the bending moment distribution in Fig. 7 (d) shows the effect of the actuator moment introduced by the PACS in active and passive mode. In passive mode, the offset in the bending moment is constant for all load cases, whereas in active mode the offset reduces with increasing loads.

The angular deflection β in Table 7 is the deflection of the actuator evaluated between the left and right nodes of the PACS beam element. A comparison with Fig. 3 (a) reveals that the angular deflections shown in Table 7 are within the stress restriction envelope for the associated pressure states. Therefore, no structural failure occurs when operating the PACS actuator under the load conditions considered in this study.

The structural model is accurate up to a beam deflection of approximately 15%, but the modeling error increases for larger deflections due to the neglect of geometric nonlinearities [28]. For the reference wing, the relative wingtip deflection in the 2.5 g maneuver is 2.0% with respect to the semi-span. The largest deflection of 4.3% with respect to the semi-span occurs for the adaptive-stiffness wing in active mode and is still within the model limits. Therefore, the model assumptions used in the VLM and the beam model are appropriate to accurately represent the aeroelastic behavior of the wing under study. Looking at the wingtips of both PACS model variants, however, the local wingtip deflections with respect to the wing segment outside the hinge line are relatively large with 20.6% (passive mode) and 33.0% (active mode). In the outer wing segment outside the hinge line, geometric nonlinearities become important and should be taken into account. Nevertheless, the effect of wingtip morphing is adequately represented in the model.

Table 7 Overview of the main results of the aeroelastic analysis for each model variant and load factor n_z. The angular deflection β and the step in wing twist $\Delta\Theta$ are evaluated between the left and right nodes of the PACS beam element. The lift L generated by the wingtip is the integral of the lift forces over the wingtip segment outboard the right node of the PACS element. The WRBM is the maximum bending moment $M_{b,\max}$ that occurs at $y = 0$, whereas $\Delta M_{b,\max}$ is the relative reduction in WRBM when comparing the PACS model variants to the reference wing.

Model variant	Load factor n_z	Angular deflection β	Step in twist $\Delta\Theta$	Lift of the wingtip L	WRBM $M_{b,\max}$	Reduction in WRBM
Reference wing	1.0	0.03°	0.0°	2143 N	$2.23 \cdot 10^5$ N m	–
	1.5	0.05°	0.0°	3215 N	$3.34 \cdot 10^5$ N m	–
	2.0	0.06°	0.0°	4287 N	$4.46 \cdot 10^5$ N m	–
	2.5	0.08°	0.0°	5359 N	$5.57 \cdot 10^5$ N m	–
PACS in passive mode	1.0	0.16°	0.1°	2113 N	$2.24 \cdot 10^5$ N m	0.3%
	1.5	2.96°	1.5°	2209 N	$3.27 \cdot 10^5$ N m	−2.2%
	2.0	5.73°	2.8°	2305 N	$4.29 \cdot 10^5$ N m	−3.7%
	2.5	8.57°	4.2°	2402 N	$5.34 \cdot 10^5$ N m	−4.2%
PACS in active mode	1.0	0.16°	0.1°	2113 N	$2.24 \cdot 10^5$ N m	0.3%
	1.5	4.89°	2.4°	1538 N	$3.21 \cdot 10^5$ N m	−3.9%
	2.0	9.86°	4.9°	873 N	$4.17 \cdot 10^5$ N m	−6.4%
	2.5	15.16°	7.5°	110 N	$5.14 \cdot 10^5$ N m	−7.8%

VI. Discussion

The following discussion focuses on the applicability of actuated adaptive wingtips under realistic operating conditions and on extending the current actuator limitations in terms of load-bearing capacity. Where available, the characteristics of the PACS-based wingtip actuator are compared to those of other wingtip devices.

The actuated adaptive wingtip concept is intended to improve the efficiency and functionalities of HAR wings, but first, the technology demonstration is being conducted on a Cessna Citation X with a low aspect ratio of about 7. While the loads acting on the wingtips of a 55 m span HAR mid-range transport aircraft exceed the load-bearing capacity of the PACS actuator [9], the actuator is capable of bearing the loads acting on the wingtips of the Cessna Citation X. The investigated actuator is geometrically designed to fit the available installation space at the wingtips of the slender HAR wing, but the geometry has not been adapted to the wing box dimensions of the Cessna Citation X. The estimated wing box dimensions of the Cessna Citation X are $h = 102$ mm and $w = 671$ mm at 90% span, which is approximately the mean spanwise position of the PACS actuator. However, the cross-sectional dimensions of the actuator are with $h = 99$ mm and $w = 675$ mm very close to the installation space available in the wing box. Therefore, only minor design modifications are required, which will have little effect on the actuator characteristics.

The aeroelastic analysis demonstrates a 4.2% and 7.8% reduction in WRBM during a 2.5 g maneuver when comparing the adaptive-stiffness hinge in passive and active mode, respectively, to the reference wing without wingtip actuator. A comparison with the literature shows that the load alleviation capability of PACS-based actuated adaptive wingtips is similar to that of other folding wingtip concepts. Wilson et al. [29] achieve a reduction in WRBM of approximately 10% to 20% under different gust and maneuver loads for a 45 m span short-range aircraft with a semi aeroelastic zero-stiffness hinge located at 80% span. In contrast, Pattinson et al. [30] show a 2% reduction in WRBM for the XRF1 aircraft in a 2.5 g maneuver. They performed numerical simulations for the aircraft equipped with a flexible hinge at about 80% of the wingspan whose stiffness of $k = 1745$ N m/° is a factor 1000 less than that of the rigid wing of the XRF1 aircraft.

A further increase in load alleviation potential of PACS actuators can be achieved in the future by extending the actuator's operating envelope, which is limited by stress peaks in the transition region between the rigid walls and the flexure hinges [9]. The very localized stress peaks imply that form optimization of the flexure hinges could significantly extend the feasible pressure domain leading to a higher load-bearing capacity of the actuator. Another possibility for

increasing the actuator's load-bearing capacity might be adding additional cell rows or scaling the cell dimensions of PACS. Increased load-bearing capacity allows the actuator to be positioned further inboard on the wing of the Cessna Citation X or to be implemented on an aircraft with a larger wingspan.

PACS actuators do not require any locking mechanism since the cruise shape of the wing is maintained by the additional actuator moment. While Airbus' semi aeroelastic hinge is locked in cruise and unlocked in gust load scenarios, the passive mode of the PACS actuator is permanently activated. In extreme load scenarios, PACS can be switched to active mode further reducing the hinge stiffness via depressurization. The depressurization with increasing loads has the same effect as a degressive-stiffness hinge. Degressive stiffness is beneficial to maintain the straight wing shape in cruise while achieving high load alleviation potential at elevated loads. Therefore, degressive stiffness is also the focus of other load alleviation concepts in the literature, which investigate degressive-stiffness wings [31, 32] or aeroelastic hinges with nonlinear spring stiffnesses [33, 34].

Moreover, active deflection of the wingtips can be realized with PACS actuators by adjusting the pressure difference between the cell rows. Active deflection enables further functionalities such as advanced flight control and mission adaptability, which will be examined in future studies. A first estimate of the actuation speed of PACS actuators shows that a full deflection (depressurization) and retraction (pressurization) cycle is possible at least at 1 Hz [16]. Higher actuation rates are likely achievable, but their evaluation requires consideration of transient fluid–structure interaction during pressurization, which was neglected in that preliminary study.

VII. Conclusion and Outlook

Folding and morphing wingtips are in the focus of research for their potential to counteract the challenges posed by high aspect ratio wings. While on-ground FWT allow aircraft to comply with the airports' space limitations, in-flight folding and morphing wingtips enable further functionalities such as load alleviation, mission adaptability, and advanced flight control. Actuated adaptive wingtips combine the functionalities of passive and active in-flight FWT by using a stiffness-adaptive aeroelastic hinge that is actively adjustable in flight. This work highlights that PACS actuators are a promising technology transforming state-of-the-art on-ground folding wingtips into multifunctional actuated adaptive wingtips with continuous shape morphing capability.

This study investigates the aeroelastic behavior of PACS-based actuated adaptive wingtips. Although the overall motivation is implementing actuated adaptive wingtips on large HAR aircraft, the technology demonstration will first be conducted on a Cessna Citation X with a span of 19.38 m. The key three results of this study are:

1) PACS are a suitable technology for use as wingtip actuators, which has been verified under realistic boundary conditions in terms of loads, installation space, and functionality. The investigated PACS actuator, which is structurally designed from glass-fiber reinforced plastic, is capable of bearing the loads acting on the wingtips of the Cessna Citation X.

2) An aeroelastic method based on a reduced beam structure coupled with VLM can efficiently evaluate the load alleviation potential of actuated adaptive wingtips. In the structural model, the PACS actuator can be implemented as an equivalent beam element and a pair of counteracting moments compensating for the initial actuator deflection due to its pressurization.

3) The PACS-based adaptive-stiffness hinge shows high load alleviation potential in a 2.5 g maneuver load case, while it maintains the straight wing shape in the 1.0 g cruise flight. Since the PACS actuator responds passively to increased loading, no unlocking or gust sensing is required to trigger load alleviation. In addition, enhanced load alleviation is possible in extreme load scenarios by switching PACS to an active mode, further reducing the hinge stiffness via depressurization. For the adaptive-stiffness hinge located on the wing of the Cessna Citation X between 86.7% and 91.2% of the semi-span, the WRBM is reduced by up to 4.2% and 7.8% in passive and active mode, compared to the reference wing without wingtip actuator.

Future research will address the extension of the simulation models used in this study. The aeroelastic analysis will be extended to include dynamic loads such as gust encounters. In addition, the use of actuated adaptive wingtips for advanced flight control through asymmetric wingtip deflection will be investigated. Replacing outboard ailerons with wingtip morphing mechanisms could solve the challenge of insufficient installation space at the tip of slender HAR wings.

The next step in realizing PACS-based actuated adaptive wingtips is the experimental proof with a functional prototype. Ongoing research investigates the integral textile manufacturing of PACS from woven glass-fiber reinforced plastic [35, 36]. The integral manufacturing of single-row cellular structures was successfully demonstrated by the authors [35]. However, PACS actuators allowing for adaptive stiffness and active deflection require two antagonistic

rows of cells. The extension of the weaving process to more complex double-row cellular structures is part of current work [36]. Considering manufacturing-specific constraints in the design process is essential for the successful realization of PACS actuators with high load-bearing capacity.

Acknowledgments

This research was funded by the Deutsche Forschungsgemeinschaft (DFG, German Research Foundation) under Germany's Excellence Strategy – EXC 2163/1-Sustainable and Energy Efficient Aviation – Project-ID 390881007 and by the German Federal Ministry for Economic Affairs and Climate Action (BMWK) under project number 20A2103D (MuStHaF).

References

[1] Afonso, F., Vale, J., Oliveira, E., Lau, F., and Suleman, A., "A review on non-linear aeroelasticity of high aspect-ratio wings," *Prog. Aerosp. Sci.*, Vol. 89, 2017, pp. 40–57. https://doi.org/10.1016/j.paerosci.2016.12.004.

[2] International Civil Aviation Organization, "Annex 14 - Aerodromes - Volume I: Aerodromes Design and Operations," , 2016.

[3] Federal Aviation Administration, "Advisory Circular - Airport Design (AC 150/5300-13A): Consolidated Change 1," , 2014.

[4] Klimmek, T., Schulze, M., Abu-Zurayk, M., Ilic, C., and Merle, A., "cpacs-MONA - An independent and in high fidelity based MDO tasks integrated process for the structural and aeroelastic design for aircraft configurations," *International Forum on Aeroelasticity and Structural Dynamics (IFASD 2019)*, Curran Associates, Red Hook, New York, 2019, pp. 430–450.

[5] American Society of Mechanical Engineers, "Wing Folding Mechanism of the Grumman Wildcat: An American Society of Mechanical Engineers Historic Mechanical Engineering Landmark," URL: https://www.asme.org/wwwasmeorg/media/resourcefiles/aboutasme/who%20we%20are/engineering%20history/landmarks/238-grumman-wildcat-sto-wing-wing-folding-mechanism.pdf, 2006. (Accessed 30 November 2022).

[6] Ajaj, R. M., "Flight Dynamics of Transport Aircraft Equipped with Flared-Hinge Folding Wingtips," *J. Aircr.*, Vol. 58, No. 1, 2021, pp. 98–110. https://doi.org/10.2514/1.C035940.

[7] Boye, S., "A passenger aircraft with a downwardly foldable wing tip device," Patent GB2524827A, 2015.

[8] Ajaj, R. M., Parancheerivilakkathil, M. S., Amoozgar, M., Friswell, M. I., and Cantwell, W. J., "Recent developments in the aeroelasticity of morphing aircraft," *Prog. Aerosp. Sci.*, Vol. 120, 2021, 100682. https://doi.org/10.1016/j.paerosci.2020.100682.

[9] Meyer, P., Traub, H., and Hühne, C., "Actuated adaptive wingtips on transport aircraft: Requirements and preliminary design using pressure-actuated cellular structures," *Aerosp. Sci. Technol.*, Vol. 128, 2022, 107735. https://doi.org/10.1016/j.ast.2022.107735.

[10] Wilson, T., Kirk, J., Hobday, J., and Castrichini, A., "Small scale flying demonstration of semi aeroelastic hinged wing tips," *International Forum on Aeroelasticity and Structural Dynamics (IFASD 2019)*, Curran Associates, Red Hook, New York, 2019, pp. 1115–1133.

[11] Wilson, T., Kirk, J., Hobday, J., and Castrichini, A., "Update on AlbatrossONE Semi Aeroelastic Hinge Small Scale Flying Demonstrator Project," *International Forum on Aeroelasticity and Structural Dynamics (IFASD 2022)*, 2022, pp. 1–22.

[12] Airbus S.A.S., "Airbus launches extra high performance wing demonstrator to fortify decarbonisation ambition," URL: https://www.airbus.com/en/newsroom/press-releases/2021-09-airbus-launches-extra-high-performance-wing-demonstrator-to-fortify, 2021. (Accessed 8 November 2022).

[13] Dussart, G. X., Lone, M., O'Rourke, C., and Wilson, T., "In-flight Wingtip Folding: Inspiration from the XB-70 Valkyrie," *Int. J. Aviat. Aeronaut. Aerosp.*, Vol. 6, No. 3, 2019, pp. 1–27. https://doi.org/10.15394/ijaaa.2019.1343.

[14] Benafan, O., Moholt, M. R., Bass, M., Mabe, J. H., Nicholson, D. E., and Calkins, F. T., "Recent Advancements in Rotary Shape Memory Alloy Actuators for Aeronautics," *Shape Mem. Superelast.*, Vol. 5, No. 4, 2019, pp. 415–428. https://doi.org/10.1007/s40830-019-00260-3.

[15] Mills, J., and Ajaj, R. M., "Flight Dynamics and Control Using Folding Wingtips: An Experimental Study," *Aerospace*, Vol. 4, No. 2, 2017, 19. https://doi.org/10.3390/aerospace4020019.

[16] Meyer, P., Lück, S., Spuhler, T., Bode, C., Hühne, C., Friedrichs, J., and Sinapius, M., "Transient Dynamic System Behavior of Pressure Actuated Cellular Structures in a Morphing Wing," *Aerospace*, Vol. 8, No. 3, 2021, 89. https://doi.org/10.3390/aerospace8030089.

[17] Pagitz, M., Lamacchia, E., and Hol, J. M. A. M., "Pressure-actuated cellular structures," *Bioinspir. Biomim.*, Vol. 7, No. 1, 2012, 016007. https://doi.org/10.1088/1748-3182/7/1/016007.

[18] Howell, L. L., *Compliant Mechanisms*, Wiley, New York, 2001.

[19] Gramüller, B., Köke, H., and Hühne, C., "Holistic design and implementation of pressure actuated cellular structures," *Smart Mater. Struct.*, Vol. 24, No. 12, 2015, 125027. https://doi.org/10.1088/0964-1726/24/12/125027.

[20] Segui, M., Bezin, S., and Botez, R. M., "Cessna Citation X Performances Improvement By An Adaptive Winglet During The Cruise Flight," *Int. J. Aerosp. Mech. Eng.*, Vol. 12, No. 4, 2018, pp. 423–430. https://doi.org/10.5281/zenodo.1316402.

[21] Segui, M., Abel, F. R., Botez, R. M., and Ceruti, A., "New Aerodynamic Studies of an Adaptive Winglet Application on the Regional Jet CRJ700," *Biomimetics*, Vol. 6, No. 4, 2021, 54. https://doi.org/10.3390/biomimetics6040054.

[22] Aviation Week Network, "Airbus X-Plane Will Test Inflight Folding Wingtips," URL: https://aviationweek.com/special-topics/sustainability/airbus-x-plane-will-test-inflight-folding-wingtips, 2021. (Accessed 8 November 2022).

[23] Delavenne, M., Barriety, B., Vetrano, F., Ferrand, V., and Salaun, M., "Parametric Analysis of an Active Winglet Concept for High Aspect Ratio Wing Using CFD/CSM Computations," *AIAA Aviation 2020 Forum*, 2020, pp. 1–17. https://doi.org/10.2514/6.2020-2662.

[24] Castrichini, A., Siddaramaiah, V. H., Calderon, D. E., Cooper, J. E., Wilson, T., and Lemmens, Y., "Preliminary investigation of use of flexible folding wing tips for static and dynamic load alleviation," *Aeronaut. J.*, Vol. 121, No. 1235, 2017, pp. 73–94. https://doi.org/10.1017/aer.2016.108.

[25] Cheung, R. C. M., Rezgui, D., Cooper, J. E., and Wilson, T., "Testing of a Hinged Wingtip Device for Gust Loads Alleviation," *J. Aircr.*, Vol. 55, No. 5, 2018, pp. 2050–2067. https://doi.org/10.2514/1.C034811.

[26] Voß, A., "Loads Kernel User Guide: DLR-IB-AE-GO-2020-136," , 2020. URL https://elib.dlr.de/140268/.

[27] Voß, A., "An Implementation of the Vortex Lattice and the Doublet Lattice Method: DLR-IB-AE-GO-2020-137," , 2020. URL https://elib.dlr.de/136536/.

[28] Bramsiepe, K., Klimmek, T., Krüger, W.-R., and Tichy, L., "Aeroelastic method to investigate nonlinear elastic wing structures," *CEAS Aeronaut J.*, Vol. 13, No. 4, 2022, pp. 939–949. https://doi.org/10.1007/s13272-022-00596-0.

[29] Wilson, T., Azabal, A., Castrichini, A., Cooper, J. E., Ajaj, R. M., and Herring, M., "Aeroelastic Behaviour of Hinged Wing Tips," *International Forum on Aeroelasticity and Structural Dynamics (IFASD 2017)*, Curran Associates, Red Hook, New York, 2017, pp. 2457–2474.

[30] Pattinson, J., Wilson, T., and Herring, M., "High Fidelity Simulation of the Folding Wing Tip for Loads Alleviaton," *International Forum on Aeroelasticity and Structural Dynamics (IFASD 2015)*, Curran Associates, Red Hook, New York, 2015, pp. 805–820.

[31] Bramsiepe, K., Braune, M., Krüger, W.-R., and Tichy, L., "Wind Tunnel Experiment with an EPP-Wing to Investigate Aeroelastic Effects of Nonlinear Elastic Stiffnesses," *33rd Congress of the International Council of the Aeronautical Sciences*, 2022, pp. 1–10.

[32] Hahn, D., and Haupt, M., "Exploration of the effect of wing component post-buckling on bending-twist coupling for nonlinear wing twist," *CEAS Aeronaut J.*, Vol. 13, No. 3, 2022, pp. 663–676. https://doi.org/10.1007/s13272-022-00586-2.

[33] Castrichini, A., Hodigere Siddaramaiah, V., Calderon, D. E., Cooper, J. E., Wilson, T., and Lemmens, Y., "Nonlinear Folding Wing Tips for Gust Loads Alleviation," *J. Aircr.*, Vol. 53, No. 5, 2016, pp. 1391–1399. https://doi.org/10.2514/1.C033474.

[34] Castrichini, A., Cooper, J. E., Wilson, T., Carrella, A., and Lemmens, Y., "Nonlinear Negative Stiffness Wingtip Spring Device for Gust Loads Alleviation," *J. Aircr.*, Vol. 54, No. 2, 2017, pp. 627–641. https://doi.org/10.2514/1.C033887.

[35] Meyer, P., Boblenz, J., Sennewald, C., Vorhof, M., Hühne, C., Cherif, C., and Sinapius, M., "Development and Testing of Woven FRP Flexure Hinges for Pressure-Actuated Cellular Structures with Regard to Morphing Wing Applications," *Aerospace*, Vol. 6, No. 11, 2019, 116. https://doi.org/10.3390/aerospace6110116.

[36] Vorhof, M., Sennewald, C., Schegner, P., Meyer, P., Hühne, C., Cherif, C., and Sinapius, M., "Thermoplastic Composites for Integrally Woven Pressure Actuated Cellular Structures: Design Approach and Material Investigation," *Polymers*, Vol. 13, No. 18, 2021, 3128. https://doi.org/10.3390/polym13183128.